Electron Localization and Delocalization in Mixed-Valence Transition Metal Clusters: Structural and Spectroscopic Studies of Oxo-Centered Trinuclear Complexes $[Fe_3O(OOCCMe_3)_6(py)_3]^{+/0}$ and $[Mn_3O(OOCCMe_3)_6(py)_3]^{+/0}$

Ruowen Wu,[†] Mehmet Poyraz,[†] Frank E. Sowrey,[†] Christopher E. Anson,[†] Sigrid Wocadlo,[†] Annie K. Powell,[†] Upali A. Jayasooriya,[†] Roderick D. Cannon,*[,†] Tadahiro Nakamoto,[‡] Motomi Katada,[‡] and Hirotoshi Sano[§]

School of Chemical Sciences, University of East Anglia, Norwich NR4 7TJ, England, Radioisotope Research Centre, Tokyo Metropolitan University, Hachioji, Tokyo 192-03, Japan, and Department of Environmental Science, School of Social Information Studies, Otsuma Women's University, Karakida, Tama, Tokyo 206, Japan

Received April 24, 1997

Crystal structures are reported for the following complexes $[Fe_3O(OOCCMe_3)_6(py)_3]ClO_4 \cdot 0.5py$, **1**; $[Mn_3O(OOCCMe_3)_6(py)_3]ClO_4 \cdot MeCN$, **2**; $[Mn_3O(OOCCMe_3)_6(py)_3]$, **4**; $[Fe_3O(OOCCMe_3)_6(py)_3]$, **5.** Crystal data are as follows: **1**, system monoclinic, space group $P2_1/n$, $a = 11.658(5)$ Å, $b = 35.450(5)$ Å, $c = 14.084(5)$ Å, $\beta = 100.10(1)°$, $V = 5730(3)$ Å^3, $Z = 4$; **2**, orthorhombic, $P2_12_12_1$, $a = 18.592(11)$ Å, $b = 25.924(11)$ Å, $c = 13.290(5)$ Å, $V = 6405(3)$ Å^3, $Z = 4$; **4**, monoclinic, $P2_1/c$, $a = 17.941(4)$ Å, $b = 14.945(3)$ Å, $c = 21.655(4)$ Å, $\beta = 96.50(3)°$, $V = 5769(2)$ Å^3, $Z = 4$; **5**, monoclinic, $P2_1$, $a = 11.800(3)$ Å, $b = 20.238(7)$ Å, $c = 12.003(2)$ Å, $\beta = 106.97(2)°$, $V = 2741.6(13)$ Å^3, $Z = 2$. In **1** and **2**, the triangular metal ion clusters are close to equilateral geometry, but the coordination polyhedra of the metal ions are significantly different. Those of the fully oxidized triiron(III) cluster are close to the ideal tetragonal symmetry. Those of the trimanganese(III) cluster show strong Jahn−Teller distortions, the four Mn−carboxylate bonds defining a long and a short O−Mn−O axis and these axes around the three Mn centers being correlated so as to define an approximate 3-fold screw axis for the whole cluster. In the mixed-valence trimanganese complex **4** the coordination implies localized valence states close to $(2Mn^{3+} + Mn^{2+})$ but in the triiron complex **5** the bond distances are close to those expected for a partially averaged state $(2Fe^{2.5+} + Fe^{3+})$. Mössbauer spectra of the mixed-valence iron complex indicate a phase transition to a localized $(2Fe^{3+} + Fe^{2+})$ state below $T = 96$ K. In the high-temperature phase, IR spectra support a model in which the electron transfer takes place between two adjacent iron centers at a rate which remains lower than that of the infrared time scale up to room temperature.

Introduction

Oxo-centered triangular complexes of the general type $[M_3O(OOCR)_6L_3]^{n+}$ are particularly valuable as frameworks for systematically studying metal−metal interactions in clusters. They have been characterized with a wide variety of first-row and heavier transition metals, with mixed-metal combinations and with mixed-valency combinations.[1] The geometry of the central cluster remains relatively constant throughout the series and is often very close to 3-fold symmetry with a planar OM_3 unit, so that quite small deviations can be highly significant. Among the issues of interest are antiferromagnetic coupling in mixed-metal clusters,[1,2] electron delocalization in mixed-valence clusters,[1,3,4] and symmetry lowering, of electronic origin, in homonuclear paramagnetic clusters.[5] A problem with the acetate series however is that most of them crystallize with extra solvent molecules which profoundly influence the physical properties.[3,4] For example, electron transfer in the mixed-valence clusters $[Fe^{III}_2Fe^{II}O(OOCMe)_6(py)_3](py)$ is accompanied by, and possibly controlled by, rotation of the extra pyridine.[3,6] It is difficult to distinguish these effects from the effects which are due to the inherent characteristics of the metal-ion cluster. On the other hand, as appears from this work, the pivalate complexes are relatively free from such problems. Although some of the "fully oxidized" salts $[M_3O(OOCCMe_3)_6L_3]X$ (where X is a monovalent anion) crystallize with small proportions of incorporated solvent, all the neutral complexes which we have examined have the simple formula $[M_2M'O(OOCCMe_3)_6L_3]$.

[†] UEA.
[‡] TMU.
[§] Otsuma Women's University.

(1) Cannon, R. D.; White, R. P. *Prog. Inorg. Chem.* **1988**, *36*, 195.
(2) White, R. P.; Stride, J. E.; Bollen, S. K.; Chaisa-Ard, N.; Kearley, G. J. K.; Jayasooriya, U. A.; Cannon, R. D. *J. Am. Chem. Soc.* **1993**, *115*, 7778.
(3) (a) Hendrickson, D. N. In *Mixed Valency Systems: Applications in Chemistry, Physics and Biology;* Prassides, K., Ed.; NATO ASI Series C: Mathematical and Physical Sciences, Vol. 343; Kluwer Academic Publications: Dordrecht, The Netherlands, 1991; pp 67−90. (b) Cannon, R. D.; Jayasooriya, U. A.; White, R. P. *Ibid.,* pp 283−298.
(4) (a) Meesuk, L.; Jayasooriya, U. A.; Cannon, R. D. *J. Am. Chem. Soc.* **1987**, *109*, 2009. (b) Meesuk, L.; White, R. P.; Templeton, B. G.; Jayasooriya, U. A.; Cannon, R. D. *Inorg. Chem.* **1990**, *29*, 2389. (c) Cannon, R. D.; Jayasooriya, U. A.; Montri, L.; Saad, A. K.; Karu, E.; Bollen, S. K.; Sanderson, W. R.; Powell, A. K.; Blake, A. B. *J. Chem. Soc., Dalton Trans.* **1993**, 2005.
(5) (a) Jayasooriya, U. A.; Cannon, R. D.; White, R. P.; Kearley, G. J. *Angew. Chem., Int. Ed. Engl.* **1989**, *28*, 930. (b) Jayasooriya, U. A.; Cannon, R. D.; White, R. P.; Stride, J. A.; Grinter, R.; Kearley, G. J. *J. Chem. Phys.* **1993**, *98*, 9303. (c) Cannon, R. D.; Jayasooriya, U. A.; Wu, R.; Arap*k*oske, S. K.; Stride, J. A.; Nielsen, O. F.; White, R. P.; Kearley, G. J.; Summerfield, D. *J. Am. Chem. Soc.* **1994**, *116*, 11869.
(6) Cannon, R. D.; Jayasooriya, U. A.; Arap*k*oske, S. K.; White, R. P.; Williams, J. H. *J. Am. Chem. Soc.* **1991**, *113*, 4158.

S0020-1669(97)00451-5 CCC: $15.00
Published on Web 03/27/1998

For these reasons, we have studied the preparative chemistry of a range of homonuclear and mixed trinuclear pivalato complexes. As result of the high solubility it has been found possible to use routes to new complexes based on redox reactions of existing complexes. Here we report a detailed comparison of four closely related complexes, involving two metals at two oxidation levels. Crystal structures and vibrational spectra indicate that the mixed-valence systems are valence-localized but in contrasting ways, the manganese system tending to the valence configuration ($2Mn^{3+} + Mn^{2+}$) but the iron system tending to ($Fe^{3+} + 2Fe^{2.5+}$), and spectroscopic data give information on internal electron-transfer rates.

Experimental Section

Preparations. $[Fe_3O(OOCC(CH_3)_3)_6(OH_2)_2(OH)]\cdot H_2O$. A solution of sodium pivalate (sodium hydroxide, 6.0 g, and pivalic acid, 15.3 g, 0.15 mol) in water (ca. 15 mL) was added with stirring to a solution of hydrated iron(III) chloride, $FeCl_3\cdot 6H_2O$, in 100 mL water. The pink or brick-red precipitate was collected, washed with 1:1 acetone−water, and dried under vacuum. Yield: 19 g. Anal. Calcd for $C_{30}H_{61}O_{17}Fe_3$: C, 41.8; H, 7.15. Found: C, 41.8; H, 7.16. IR spectrum: a peak at 3600 cm^{-1}, OH^- stretch. The product deteriorates on prolonged standing in air, becoming redder in color and not completely soluble in pyridine.

$[Fe_3O(OOCC(CH_3)_3)_6(C_5H_5N)_3]ClO_4\cdot 0.5C_5H_5N$ (1). The above product (6 g, 7.0 mmol) was dissolved with warming in pyridine (16 mL), and either $[n\text{-}Bu_4N]ClO_4$ (8 g) or anhydrous $NaClO_4$ (3 g) was added slowly with stirring. After cooling, the brown-green crystals were collected, recrystallized from pyridine (3 g in 10 mL), and finally washed with 1:1 acetone−water and dried under vacuum. Anal. Calcd for $C_{45}H_{69}N_3O_{17}Fe_3Cl$: C, 7.9; H, 6.17; N, 3.73; Cl, 3.15. Found: C, 47.9; H, 6.19; N, 3.65; Cl, 3.21. The method works equally well at four times the scale. Crystal morphology was found to be highly dependent on the speed of crystallization, and although analytically acceptable products were obtained after 1 day, the best crystals were obtained with slow cooling and evaporation over 1 week, in open air, in which case no recrystallization was necessary. The X-ray crystal structure (below) indicates the presence of uncoordinated pyridine (estimated, 0.5 molecules per unit of trinuclear complex), but this was not apparent in the chemical analysis.

$[Mn_3O(OOCC(CH_3)_3)_6(C_5H_5N)_3][ClO_4]\cdot CH_3CN$ (2). The mixed-valence complex **4** (1.0 g, 1 mmol) was dissolved in 40 mL of acetonitrile, and silver perchlorate (0.2 g, 1 mmol) was added. The mixture was stirred in darkness for 2 h. After metallic silver (a black powdery deposit) had been filtered off, the solution was left to evaporate, in open air, in darkness, at room temperature. After about 20 days, brown crystals were collected and recrystallized three times from acetonitrile. Anal. Calcd for $C_{45}H_{69}N_3O_{17}Mn_3Cl$: C, 48.1; H, 6.19; N, 3.74. Found: C, 47.8; H, 6.03; N, 3.60. A good-quality product is pale brown in color. If it is not isolated quickly the more stable, black, mixed-valence $Mn^{III}_2Mn^{II}$ product forms on prolonged contact with pyridine. The X-ray crystal structure (below) indicates the presence of uncoordinated acetonitrile (estimated, 1 molecule per unit of trinuclear complex), but this was not apparent in the chemical analysis or IR spectra of bulk material; e.g., there was no C−N stretch band at ca. 2200 cm^{-1}. Before the above method was discovered, the following was used. Hydrated manganese(II) chloride, $MnCl_2\cdot 4H_2O$ (4.0 g), and potassium permanganate (0.83 g) were added to a mixture of pivalic acid (10 g) and sodium hydroxide (2.5 g) in 10 mL water. After being warmed and stirred for 3 h, the mixture was allowed to cool, and the product was rapidly recrystallized from dichloromethane containing a slight excess of pyridine and tetra-*n*-butylammonium perchlorate. This gave authentic products but lower yields.

$[Mn_3O(OOCC(CH_3)_3)_6(C_5H_5N)_3]BF_4$ (3). The mixed-valence manganese complex **4** (0.55 g, 0.5 mmol) and silver tetrafluoborate, $AgBF_4$ (0.105 g, 0.5 mmol), were dissolved in 65 mL of dry dichloromethane, and the solution was stirred in the dark at room temperature for 5 h. After silver had been filtered off as before, the solution was divided into two equal portions in cylindrical specimen tubes, and the tubes were placed inside tightly stoppered bottles containing carbon tetrachloride. After 2 days of standing in darkness at room temperature, the product, consisting of brown needle-shaped crystals, was collected and washed with diethyl ether to remove excess $AgBF_4$. Anal. Calcd for $C_{45}H_{69}N_3O_{13}Mn_3BF_4$: C, 48.6; H, 6.26; N, 3.78. Found: C, 50.5; H, 6.48; N, 3.72.

$[Mn_3O(OOCC(CH_3)_3)_6(py)_3]$ (4). To a mixture of ground manganese(II) chloride tetrahydrate, $MnCl_2\cdot 4H_2O$ (8.8 g, 44 mmol), and finely ground potassium permanganate, $KMnO_4$ (0.80 g, 5 mmol), in a 250 mL conical flask, a mixture of molten pivalic acid (60 mL) and pyridine (40 mL) was added, followed by 20 mL of water. The deep-brown (almost black) mixture was heated with continuous stirring, at 50−55 °C for 4 h. The mixture was filtered, and the black solid was washed extensively with water and dried in air. Small shiny black crystals were isolated, typical yield 2.7 g, 15.6%. Anal. Calcd for $C_{45}H_{69}Mn_3N_3O_{13}$: C, 52.7; H, 6.79; N, 4.10; total Mn, 16.07; Mn(III), 10.72. Found: C, 53.0; H, 6.67; N, 4.09; total Mn, 16.8; Mn(III), 11.25; Cl, below detection limit. The product can be recrystallized by dissolving in pyridine at room temperature and allowing the solution to evaporate in air.

$[Fe_3O(OOCC(CH_3)_3)_6(HOOCC(CH_3)_3)_3]$. To a solution of iron(II) chloride, $FeCl_2\cdot 4H_2O$ (13 g, 54 mmol), in water (50 mL) was added a mixture comprising pivalic acid (32 g, 0.31 mol), sodium pivalate (6.5 g, 0.16 mol), dimethyl ethylene glycol (10 mL), and water (10 mL). The mixture was refluxed for 1 h and then left in the flask open to air. A black crystalline solid formed in the upper organic layer, and the aqueous phase was colorless. Oxygen was not excluded during the refluxing, but it was noted that, for a successful preparation, the organic phase should remain almost black in color, whereas with excessive oxygen this phase became brown and an iron(III) product was formed. The solid was filtered off and washed under nitrogen, with deoxygenated 1:1 acetone−water, then dried in a stream of dry nitrogen, and stored under nitrogen. Anal. Calcd for $C_{45}H_{84}O_{19}Fe_3$: C, 49.3; H, 7.22; Fe, 15.3. Found: C, 49.0; H, 7.85; Fe, 14.71. The IR spectrum in the region 800−400 cm^{-1} is consistent with the oxo-centered trinuclear structure.

$[Fe_3O(OOCC(CH_3)_3)_6(C_5H_5N)_3]$ (5). The preceding pivalic acid adduct (3 g) was recrystallized from pyridine (6 mL) in the absence of oxygen. Shiny black crystals were collected, washed with 1:1 acetone−water, and dried and stored under nitrogen. Anal. Calcd for $C_{45}H_{69}N_3O_{13}Fe_3$: C, 52.6; H, 6.72; N, 4.09; Fe total, 16.3; iron(II), 5.44. Found: C, 52.8; H, 6.91; N, 3.92; Fe total, 15.7; iron(II), 5.17.

Perdeuteriopyridine analogues of **1** and **3**−**5** were prepared by the same methods, using C_5D_5N in place of C_5H_5N.

Analyses. Manganese(III) was determined by adding a standardized aliquot of 0.1 M ammonium iron(II) sulfate in 1 M H_2SO_4 to a weighed solid sample in a dry vessel. The solution was heated cautiously to complete the reduction. The mixture was cooled to room temperature, and excess iron(II) was potentiometrically titrated with cerium(IV). To determine total manganese, manganese(III) was reduced to manganese(II) by boiling a solution of complex (ca. 50 mg) and hydroxylamine hydrochloride (0.5 g) in 25 mL of water for about 2 min. After reduction was complete (colorless solution), pH was adjusted by the addition of 2 mL of a buffer solution prepared by mixing 8 g of ammonium nitrate and 35 mL of concentrated aqueous ammonia (S.G. 0.880) in 65 mL of water. The solution was titrated with Na_2H_2edta solution using pyrocatechol violet (color change, blue to violet) or Eriochrome Black T (red to blue) as indicator. Manganese(II) in the presence of iron(III) was determined by the same procedure with triethanolamine as a masking reagent. Total iron was determined by dissolving the complex in acetonitrile−water, reducing with amalgamated zinc, filtering, and titrating with cerium(IV). Iron(II) was determined by a spectrophotometric titration with bromine in CH_2Cl_2. The bromine solution was standardized by reacting with excess aqueous KI and titrating with thiosulfate.

Warning. *Anhydrous metal perchlorate salts were assumed to be dangerously explosive until proved otherwise. They were stored only in small amounts, were not heated, and were not scraped with metal spatulas on glass sinters.* In fact, no problems were experienced with the materials reported here. In careful tests, small amounts of solid burned quietly on an open spatula and were heated in test tubes without

Table 1. Crystallographic Data and Structure Determination Summaries

	1	**2**	**4**	**5**
empirical formula	$C_{47.5}H_{71.5}Fe_3N_{3.5}O_{17}Cl$	$C_{47}H_{72}Mn_3N_4O_{17}Cl$	$C_{45}H_{69}Mn_3N_3O_{13}$	$C_{45}H_{69}Fe_3N_3O_{13}$
fw	1166.59	1165.36	1024.85	1027.60
color	dark brown	brown	black	dark brown
cryst size (mm)	0.60 × 0.30 × 0.30	0.20 × 0.15 × 0.02	0.7 × 0.5 × 0.5	0.30 × 0.30 × 0.20
cryst system	monoclinic	orthorhombic	monoclinic	monoclinic
space group	$P2_1/n$	$P2_12_12_1$	$P2_1/c$	$P2_1$
a (Å)	11.658(5)	18.592(11)	17.941(4)	11.800(3)
b (Å)	35.450(5)	25.924(11)	14.945(3)	20.238(7)
c (Å)	14.084(5)	13.290(5)	21.655(4)	12.003(2)
β (deg)	100.10(1)		96.50(3)	106.97(2)
V (Å^3)	5730(3)	6406(5)	5769(2)	2741.6(13)
Z	4	4	4	2
ρ_{calc} (Mg m^{-3})	1.329	1.208	1.180	1.245
μ (mm^{-1})	0.861	0.864	0.700	0.837
F(000)	2448	2440	2156	1084
radiation	Mo Kα	Mo Kα	Mo Kα	Mo Kα
T (K)	293(2)	233(2)	293(2)	293(2)
reflcns collcd	14 202	4213	9693?	9842
unique reflcns	6820	4213	9693	5003
reflcns used	6819	4213	9684	4445 ($F > 2\sigma(F)$)
abs corr				ψ-scans (0.788 > T > 0.699)
refinement on	F^2	F^2	F^2	F
params refined	638	662	676	582
wR_2 (all data)	0.1138	0.1714	0.2084	
R_1 ($I > 2\sigma(I)$)[a]	0.0439	0.0549	0.0521	
R ($F > 2\sigma(F)$)[b]				0.0699
wR ($F > 4\sigma(F)$)[b]				0.0919
S[c]	1.059	1.051	1.075	0.91
largest diff peak and hole (e Å^{-3})	0.617, −1.007	0.570, −0.327	0.589, −0.481	0.44, −0.44

[a] All data used in refinement; criterion only applied in calculation of "conventional" *R*-factor after refinement. [b] Refinement using observed reflections only. [c] Based on all data for **1**, **2**, and **4** and on observed data for **5**.

explosion. Analyses for C, H, and N were carried out by combustion, and those for Cl, by silver ion titration after combustion, in the usual way.

X-ray Crystallography. Crystal data and data collection procedures are summarized in Table 1. Unit cell parameters were refined from the setting angles of 25 centered reflections. All operations were carried out in air. The iron mixed-valence complex **5** is air-sensitive, but in the solid-state decomposition is very slow. A loss of intensity of 9.5% was observed during the 8 days of data collection, and the data were scaled accordingly. Reflections were corrected for Lorentz and polarization effects and for absorption. In all four materials the complex molecules were found to lie on general sites in the unit cell, with one molecule in the asymmetric unit. Structures were solved by direct methods using the Shelxtl Plus software package. Carbon occupancies of disordered groups were refined and then fixed for subsequent refinements. In **5**, which has all six *tert*-butyls disordered, the C−CH_3 distances were constrained to 1.54(3) Å. All non-hydrogen atoms except for the disordered ones were assigned anisotropic temperature factors. Hydrogens were placed in calculated positions. The structures were then refined to convergence. Structures **2** and **5** are noncentric: The absolute configuration of the unit cell was confirmed for **2** by means of the Flack χ parameter, and that for **5**, by noting that refinement of the inverted cells led to higher residuals. Atomic coordinates, bond distances and angles, anisotropic displacement coefficients, and occupancy factors are listed in Tables S1-S17. Molecular structures are shown in Figures 1−4. Selected bond distances are compared in Table 2.

IR Measurements. Spectra were obtained using KBr disks, on a Perkin-Elmer 684 grating spectrophotometer and on a Unicam Mattson 5000 FTIR spectrometer with resolution 1 cm^{-1} (128 scans).

Mössbauer Measurements. Spectra for ^{57}Fe were obtained using a constant-acceleration type spectrometer, over the temperature range 8.4−298 K. Observed spectra were fitted to Lorentzian line shapes by a least-squares procedure. Velocity calibration was done by measuring absorption lines of an iron foil sample against a ^{57}Co(Rh) source. All isomer shifts were referred to metallic Fe. Spectral parameters—isomer shifts and quadrupole splittings—and curve-fitting parameters are listed in Table S18.

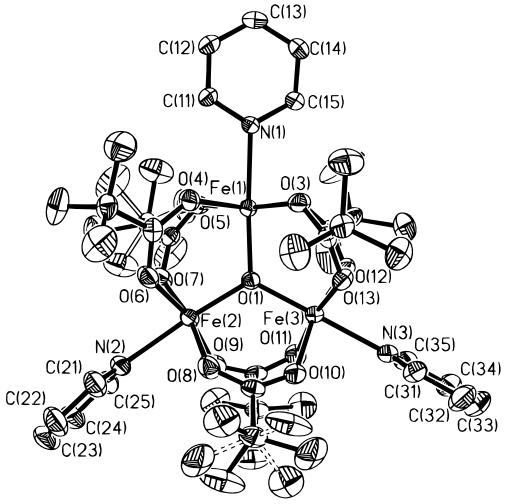

Figure 1. Structure of the complex cation in $[Fe_3O(OOCCMe_3)_6(py)_3]$-$ClO_4$·0.5py (**1**) with thermal ellipsoids drawn at the 90% probability level. (Hydrogen atoms and numbers of some atoms are omitted for clarity.)

Results

Structures. $[Fe^{III}_3O(OOCCMe_3)_6(py)_3]ClO_4$·0.5py (1) (Figure 1). Within experimental error, the central Fe_3O unit has 3-fold symmetry and the oxygen lies almost in the same plane as the three metal atoms. The metal atoms all have very similar, nearly octahedral ligand environments: The average value and the spread of values (expressed here as mean ± standard deviation) of the three iron-central oxygen distances are 1.905 ± 0.004 Å, and those of the three iron−nitrogen distances, 2.186 ± 0.020 Å. For the four iron−carboxylate distances surrounding each iron atom, averages and standard deviations are as follows: Fe1, 2.012 ± 0.005; Fe2, 2.014 ± 0.005; Fe3, 2.006

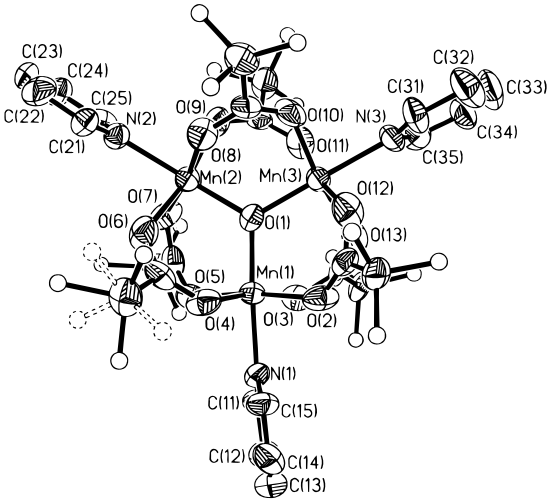

Figure 2. Structure of the complex cation in $[Mn_3O(OOCCMe_3)_6(py)_3]ClO_4 \cdot CH_3CN$ (**2**) with thermal ellipsoids drawn at the 90% probability level. (Hydrogen atoms and numbers of some atoms are omitted for clarity.)

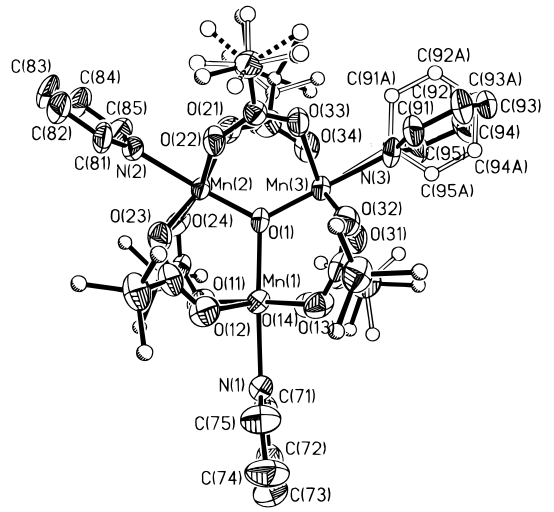

Figure 3. Structure of complex $[Mn_3O(OOCCMe_3)_6(py)_3]$ (**4**) with thermal ellipsoids drawn at the 90% probability level. (Hydrogen atoms and numbers of some atoms are omitted for clarity.)

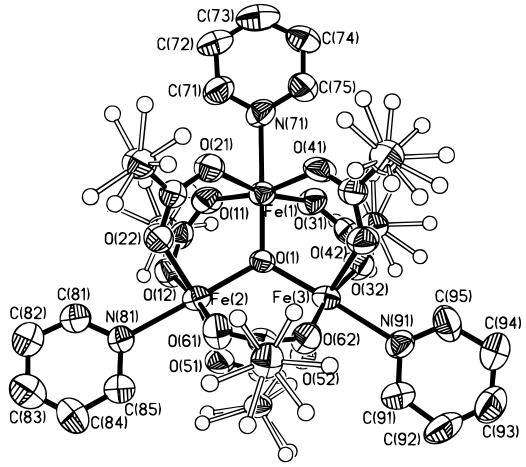

Figure 4. Structure of complex $[Fe_3O(OOCCMe_3)_6(py)_3]$ (**5**) with thermal ellipsoids drawn at the 90% probability level. (Hydrogen atoms and numbers of some atoms are omitted for clarity.)

Table 2. Selected Bond Lengths for $[M_3(\mu_3\text{-}O)(\mu_2\text{-}O_2CCMe_3)_6(C_6H_5N)_3]^{n+}$ (M = Fe, Mn; n = 1, 0)

	compd			
	1 (Fe_3O^+)	**2** (Mn_3O^+)	**4** (Mn_3O)	**5** (Fe_3O)
M1−O1	1.903(3)	1.896(8)	2.171(3)	1.841(6)
M2−O1	1.902(3)	1.867(8)	1.813(3)	1.954(6)
M3−O1	1.910(2)	1.909(8)	1.848(3)	1.920(6)
M1−N1	2.163(3)	2.061(10)	2.339(4)	2.257(10)
M2−N2	2.209(4)	2.080(10)	2.105(4)	2.221(8)
M3−N3	2.185(3)	2.112(10)	2.109(7)	2.238(9)
M1−O	2.012(3)	2.145(9)	2.148(4)	2.023(9)
M1−O	2.006(3)	1.936(8)	2.168(4)	2.047(7)
M1−O	2.009(3)	1.940(9)	2.202(4)	2.015(6)
M1−O	2.020(3)	2.155(8)	2.170(4)	2.007(10)
M2−O	2.005(3)	2.134(10)	2.223(4)	2.048(8)
M2−O	2.014(3)	1.920(8)	1.989(3)	2.106(9)
M2−O	2.019(3)	1.941(9)	2.181(4)	2.045(7)
M2−O	2.017(3)	2.130(9)	1.977(3)	2.078(9)
M3−O	2.007(3)	2.140(9)	2.143(4)	2.043(9)
M3−O	2.024(3)	1.937(9)	1.997(4)	2.112(9)
M3−O	1.997(3)	1.915(8)	2.193(4)	2.053(8)
M3−O	1.996(3)	2.100(10)	2.004(4)	2.037(7)
O1−M_3 plane	0.009(4)	0.002(7)	0.012(3)	0.001(7)

± 0.011 Å. Thus the standard deviations for the sets are approximately twice or three times the average esd for the individual bond lengths. The C−O distances in the carboxyl groups are all very similar, 1.257 ± 0.012 Å, with no significant tendency toward unequal distances in any carboxyl group and no apparent pattern of long or short distances in relation to the structure of the complex. The most obvious deviations from 3-fold symmetry of the cluster as a whole is that two of the coordinated pyridine molecules are set approximately perpendicular to the triiron plane while the third is nearly coplanar and that two of the six *tert*-butyl groups are disordered. The only other disorders, apart from presumed rotational disorders of methyl groups, concern the perchlorate ion, slightly disordered between two closely neighboring positions, and the noncoordinated pyridines. These amount to approximately 0.5 molecules per molecule of trimer and are located with 2-fold disordering with their centroids at the inversion center, $^1/_2$, $^1/_2$, $-^1/_2$.

$[Mn_3O(OOCCMe_3)_6(py)_3]ClO_4 \cdot MeCN$ (2) (Figure 2). Although the molecules occupy general sites and thus have no internal symmetry, the central Mn_3O cluster approximates fairly closely to 3-fold symmetry. Within experimental error the central oxygen lies in the plane of the metal atoms, and all three metal atoms show similar coordination, though the small differences are outside the limits of experimental error. For example the distances, Mn to central oxygen, are as follows: Mn1−O, 1.896(8); Mn2−O, 1.867(8); Mn3−O, 1.909(8) Å. The planes of the coordinated pyridines are nearly at right angles to that of the central Mn_3O cluster. The patterns of coordination to the carboxylate oxygens are also similar but not regular: each metal ion has the expected Jahn−Teller distortion, with two longer and two shorter Mn−O bonds, the long pair and the short pair forming a long and a short axis in pseudo-octahedral coordination. The orientations of the long and short axes through the metal centers are related by an approximate 3-fold axis through the center of the molecule. In other words, with reference to Figure 2, the longer O−Mn−O axes are the vectors O2→O5, O6→O9, and O10→O13. Each of the six bridging carboxylate groups participates in one long and one short Mn−O bond, and the C−O bond distances within each carboxylate differ significantly, the longer C−O distances linking to the shorter Mn−O distance and vice versa. The perchlorate ions in this structure occupy ordered sites, but an acetonitrile

molecule is disordered over two positions with occupancies 0.51, 0.49, i.e., equal occupancies within experimental error.

$[Mn_3O(OOCCMe_3)_6(py)_3]$ (4) (Figure 3). Two of the metal atoms show very similar coordination, i.e., Mn2 and Mn3, while Mn1 is distinctly different from these two. For Mn2 and Mn3, the manganese−central oxygen bond distances are similar within experimental error, 1.813(3) and 1.848(3) Å; for Mn1 it is significantly longer, 2.171(3) Å. Similarly the metal−nitrogen distances are as follows: Mn1, 2.339(4); Mn2, 2.105(4); Mn3, 2.109(7) Å. The four metal−carboxylate oxygen distances surrounding Mn1 are all similar, mean and standard deviation being 2.172 ± 0.019 Å, but the distances for Mn2 and Mn3 show collinear pairs of longer (2.185 ± 0.029 Å) and of shorter (1.972 ± 0.038 Å) bonds, and the orientations of the longer and shorter O−Mn−O axes are related in the same way as each pair of such axes in the trimanganese(III) compound. Conversely the carboxylate groups bridging Mn2 and Mn3 have long and short C−O distances, the oxygen with the longer C−O having the shorter Mn−O distance and vice versa. In other words, the coordination groups around the manganese atoms are entirely consistent with assignments of whole number oxidation states, Mn1 as manganese(II) and Mn2 and Mn3 as manganese(III). Two of the coordinated pyridines are almost perpendicular to the trimanganese plane, and the third is disordered between approximately coplanar and perpendicular orientations. But in this respect the approximate 2-fold symmetry of the central cluster is not followed, since the disordered pyridine belongs to Mn3 and not to Mn1.

$[Fe_3O(OOCCMe_3)_6(py)_3]$ (5) (Figure 4). In the analogous acetate compound, the molecules are located on sites of crystallographic 3-fold symmetry, so that the three iron atoms are indistinguishable,[8] and this is attributed to dynamic disordering resulting from rapid internal electron transfer. In the present compound, the molecules occupy a general site. The central Fe_3O cluster however approximates fairly closely to C_{2v} symmetry. Within experimental error, the central oxygen lies in the plane of the three metal atoms. Two of the metal atoms, Fe2 and Fe3, have very similar coordination and are distinct from the third, Fe1. The mean and the standard deviation of the four metal−acetate distances in each case are as follows: Fe1, 2.023 ± 0.015; Fe2, 2.069 ± 0.025; Fe3, 2.061 ± 0.029 Å. The first of these mean values is close to typical values for iron(III)−oxygen; the other two are intermediate between the typical Fe(III)−O and Fe(II)−O distances. On this basis it seems that the triiron cluster approximates to the combination of one center of valency 3 and two nearly equivalent centers with average valency 2.5. The other bond distances about the iron atoms show an interesting anomaly. Distances to the central oxygen are again one short and two long (Fe1−O, 1.841; Fe2−O, 1.954; Fe3−O, 1.920 Å), but iron−nitrogen distances are the other way round (Fe1−N, 2.257; Fe2−N, 2.221; Fe3−N, 2.238 Å). This type of inversion has been seen in another oxo-centered mixed-valence complex, $[Fe^{III}_2Fe^{II}O(OOCMe)_6(3\text{-}Mepy)_3](CH_3C_6H_5)$. In that case the metal−acetate distances showed the "normal" pattern approximating to two Fe(III) and one Fe(II), but again the longer metal−central oxygen bond was opposite to the shorter metal−pyridine bond and vice versa.[9] As regards the carboxylate ligands, the two C−O bond distances within each ion are equal within ±0.025 Å and not correlated with the different valencies. The only significant disordering in the structure concerns rotation of the *tert*-butyl groups (and no doubt of the methyl groups, but no attempt was made to ascertain this).

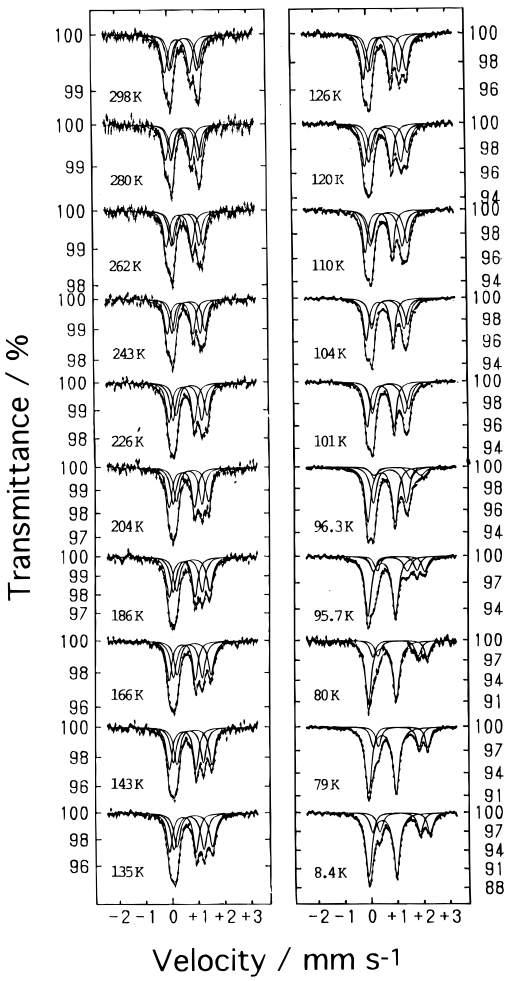

Figure 5. Mössbauer spectra of compound $[Fe_3O(OOCCMe_3)_6(py)_3]$ (**5**).

In all four complexes, the central oxygen atoms are very close to the plane of the three metals. In two cases, **2** and **5**, the estimated distance is less than the esd (see Table 2), and it may be significant that these are the two complexes in which the orientations of the three coordinated pyridines with respect to the plane are similar (approximately perpendicuar and approximately coplanar, respectively). There is a clear contrast between the fully oxidized iron(III) complex **1**, reported here, and the pivalate-bridged triiron(III) complex $[Fe_3O(OOCCMe_3)_6(MeOH)_3]Cl$ in which the corresponding distance is 0.24 Å.[9a]

Mössbauer Spectra. Mössbauer spectra of the mixed-valence iron complex **5** are displayed in Figure 5, over the temperature range 8.4−298 K. It is clear that there is a phase transition over the range 96−101 K, with sharply distinct structural regimes above and below these temperatures. At low temperature, the high-velocity components of two iron(II) doublets can be distinguished, but only one iron(III) doublet can be seen. The area ratios are close to 4:1:1 $Fe^{III}/Fe^{II}(A)/Fe^{II}(B)$. Above the phase transition the band pattern is consistent with one iron(III) center and two others with similar but not identical spectral parameters, approximating to fractional oxida-

(7) Vogel, A. I. *A Textbook of Quantitative Inorganic Analysis*, 3rd ed.; Longman: London, 1961.
(8) Woehler, S. E.; Wittebort, R. J.; Oh, S. M.; Kambara, T.; Hendrickson, D. N.; Inniss, D.; Strouse, C. E. *J. Am. Chem. Soc.* **1987**, *109*, 1063.
(9) (a) Oh, S. M.; Wilson, S. R.; Hendrickson, D. N.; Woehler, S. E.; Wittebort, R. J.; Inniss, D.; Strouse, C. E. *J. Am. Chem. Soc.* **1987**, *109*, 1073. (b) Blake, A. B.; Fraser, L. R. *J. Chem. Soc., Dalton Trans.* **1975**, 193.

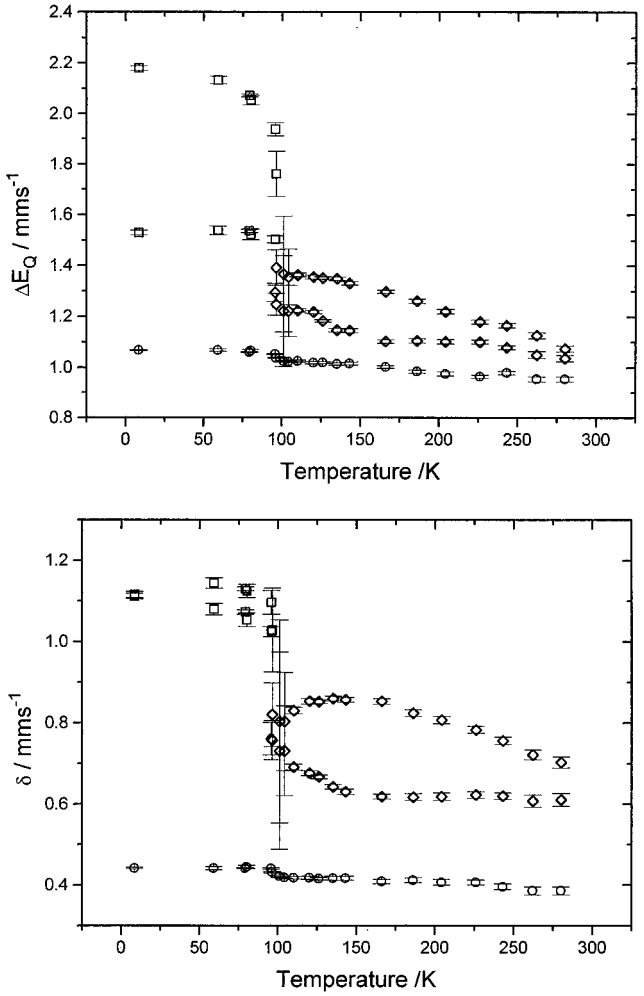

Figure 6. Temperature dependence of Mössbauer spectral parameters of compound $[Fe_3O(OOCCMe_3)_6(py)_3]$ (**5**): (a, top) isomer shifts; (b, bottom) quadrupole splittings. Points ○ are assigned to resonances of Fe^{3+}, points □, to Fe^{2+}, and points ◊, to $Fe^{\approx 2.5+}$.

tion states 2.5. Isomer shifts and quadrupole splittings (listed in Table S18) are plotted against temperature in Figure 6. We propose that below the phase transition there are two sets of structurally distinct molecules, both with the fully localized electronic configuration $Fe^{III}_2Fe^{II}$. The iron(II) centers of the two sets are different enough to be resolved in the spectra, but all four iron(III) centers of the two sets are indistinguishable within the resolution of the spectra. In the high-temperature phase, the spectral parameters are consistent with the room-temperature crystal structure. Although the general appearance of the spectra from 120 to 298 K might suggest motional narrowing with increasing temperature, the curve fits do not support this. All the bandwidths remain essentially unchanged (Table S18). It is only the quadrupole splittings of the two doublets having partial iron(II) character which change, decreasing with increasing temperature as expected for high-spin iron(II).

Changes from localized to delocalized character, on the Mössbauer time scale, without change in bandwidth, have been noted in some other mixed-valence iron materials. In some biferrocenium salts,[11−16] and in one acetate-bridged oxo-

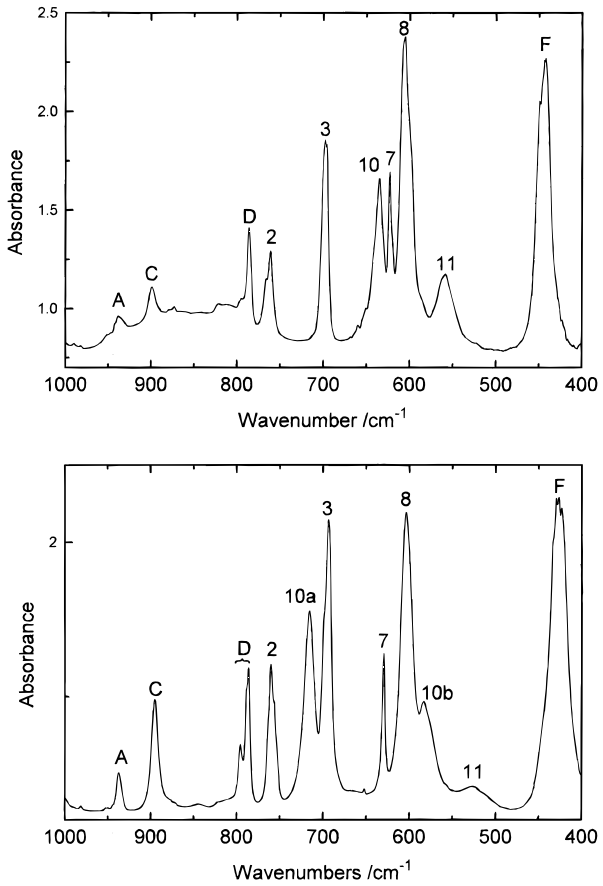

Figure 7. IR spectra of (a, top) $[Fe_3O(OOCCMe_3)_6(py)_3]ClO_4 \cdot 0.25py$ (**1**) and (b, bottom) $[Fe_3O(OOCCMe_3)_6(py)_3]$ (**5**) (KBr disks, $T = 80$ K; resolution 1 cm^{-1}).

trinuclear complex,[17] quadrupole-split doublets of iron(II) and iron(III) converge into each other with increasing temperature, without appreciable broadening, and finally become one doublet assignable to the averaged-valence state.

Vibrational Spectra. Infrared spectra of the oxidized and mixed-valence iron complexes **1** and **5** are compared in Figure 7. Frequencies and assignments are listed in Table 3. Bands due to coordinated pyridine were identified by comparisons with the respective perdeuteriopyridine complexes and with previously reported complexes of similar structure.[18] Most of the bands due to vibrations of pivalate ion were identified by comparisons involving free pivalic acid and its sodium salt, using previous discussions in the literature. Longueville *et al.*[19] have given assignments of the pivalate group based on Raman

(10) Wells, A. F. *Structural Inorganic Chemistry*, 4th ed.; Clarendon Press: Oxford, U.K. 1975; p 734.
(11) Nakashima, S. *Nucl. Inst. Methods Phys. Res.* **1993**, *B96*, 4508.
(12) Sano, H. *Hyperfine Interact.* **1990**, *53*, 97.
(13) Iijima, S.; Saida, R.; Motoyama, I.; Sano, H. *Bull. Chem. Soc. Jpn.* **1981**, *54*, 1375.
(14) Dong, T.-Y.; Hendrickson, D. N.; Iwai, K.; Cohn, M. J.; Geib, S. J.; Rheingold, A. L.; Sano, H.; Motoyama, I.; Nakashima, S. *J. Am. Chem. Soc.* **1985**, *107*, 7996.
(15) Nakashima, S.; Katada, M.; Motoyama, I.; Sano, H. *Bull. Chem. Soc. Jpn.* **1986**, *59*, 2923.
(16) Nakashima, S.; Masuda, Y.; Motoyama, I.; Sano, H. *Bull. Chem. Soc. Jpn.* **1987**, *60*, 1673.
(17) Oh, S. M.; Hendrickson, D. N.; Hasset, K. L.; Davis, R. E. *J. Am. Chem. Soc.* **1985**, *107*, 8009.
(18) (a) Johnson, M. K.; Powell, D. B.; Cannon, R. D.; *Spectrochim. Acta* **1981**, *37A*, 995. (b) Montri, L.; Cannon, R. D. *Spectrochim. Acta* **1985**, *41A*, 643. (c) Meesuk, L.; Jayasooriya, U. A.; Cannon, R. D. *Spectrochim. Acta* **1987**, *43A*, 687. (d) White, R. P.; Chai-Sa'ard, N.; Bollen, S. K.; Cannon, R. D.; Jayasooriya, U. A.; Robertson, S. T.; Steigenberger, U.; Tomkinson, J. *Spectrochim. Acta* **1990**, *46A*, 903. (e) Anson, C. E.; Chai-Sa'ard, N.; Bourke, J. P.; Cannon, R. D.; Jayasooriya, U. A.; Powell, A. K. *Inorg. Chem.* **1993**, *32*, 1502.
(19) Longueville, W.; Fontaine, H. *J. Raman Spectrosc.* **1978**, *7*, 238.

Table 3. IR Band Frequencies (cm^{-1}) and Assignments

band	**1** ($Fe_3O^+ClO_4^-$ salt)	**3** ($Mn_3O^+BF_4^-$ salt)	**5** (Fe_3O mixed-valence)	**4** (Mn_3O mixed-valence)	assgnt
A	938 br	950, 938	937	945, 935	$\gamma(CH_3) + \nu(CC_3)$
C	898, 888	896	894	895, 889	$\gamma(CH_3)$
D	785	797, 785	796, 786	795, 788	$\nu(C-CO_2)$
2	762	767	755	767, 759, 751	py(ν_4), τ(ring)[a]
W		743			$BF_4^-(\nu_1)$[d]
10a			715	705[b]	$\nu_{as}(M_3O)$
3	699	694	695	696	py(ν_{11}), γ(CH)[a]
10	635	obs			$\nu_{as}(M_3O)$
X	obs				$ClO_4^-(\nu_4)$[d,e]
5	obs	635	obs	630	$\delta(CO_2)$
7	623		627		py(ν_{6a}), δ(ring)[a]
		648		644	
8	604	596, 583	603	596, 587	$\pi(CO_2)$
				570	*c*
10b			582	obs	$\nu_{as}(M_3O)$
11	557	556	539	551, 538	$\rho_t(CO_2)$
Y		534, 521			$BF_4^-(\nu_4)$[d]
F	443	462, 457	429	448	δ(CCC)
13	obs	436	obs	435	py(ν_{16b}), τ(ring)[a]

[a] Pyridine modes numbered according to ref 23e: see also ref 23 g. [b] Perdeuteriopyridine complex. [c] Presumed to be a component of 8 or 11. [d] Reference 26. [e] Expected at 625 cm^{-1}.

spectra and normal coordinate analysis.[20] They consider that most of the observed bands are due to mixtures of several normal modes but that, in many cases, a "visualization" based on calculated atomic displacements justifies the familiar descriptions as "C−C stretch", etc. In Figure 7a, band D at 785 cm^{-1} is asssigned mainly to the C−C stretch, $\nu(C-CMe_3)$, shifted from $\nu(C-CH_3) = 950$ cm^{-1} in the corresponding acetate complexes. The strong band 8 at 604 cm^{-1} is assigned to a coincidence of the angle deformation δ(OCO), shifted from ca. 650 cm^{-1} in the acetates, and the out-of-plane deformation $\pi(CO_2)$, shifted from 620 cm^{-1} in the acetates. The most difficult assignment in this region has been the relatively weak band 11. A similar band was seen in the acetates but not in some other carboxylates such as trichloroacetates.[21] It varies in intensity and frequency between different complexes in a puzzling fashion and was liable to be confused with one of the components of $\nu_{as}(Fe_3O)$ until a series of definitive measurements settled the assignment. Isotopic substitution of central oxygen by ^{18}O identified $\nu_{as}(Fe_3O)$ and $\nu_{as}(Fe_2NiO)$ in acetate complexes,[18b,c] and inelastic neutron scattering spectra[18d] showed that band 11 was a vibration of the carboxylate ion, evidently the in-plane angle deformation or alkyl rocking mode $\rho_r(RCO_2)$, R = Me. In the Raman spectrum of pivalic acid, a band at 524 cm^{-1} has been assigned to a related C−C−C deformation.[19,20] Any explanation of why this "mystery band"[1] 11 should vary so much in frequency and intensity will depend on a future, more detailed analysis.

These analyses leave one broad band 10, in the fully iron oxidized complex, and two broad bands 10a and 10b, in the mixed-valence iron complex, assigned to the asymmetric in-plane-stretch $\nu_{as}(Fe_3O)$. In the triiron(III) complex band 10 is partly obscured at room temperature by the pyridine mode 7, but it is distinct in the spectrum recorded at low temperature with the highest available resolution (Figure 7a) and was seen more clearly still when the pyridine band was shifted by deuteration. The same applies to band 10a for the mixed-valence complex**.** It is overlapped by a different pyridine mode 3, but is resolved in Figure 7b and was fully separated in the deuteriopyridine complex. The definitive assignment of bands 10a and 10b comes from the temperature-dependence of frequency and bandwidth,[22] discussed further below.

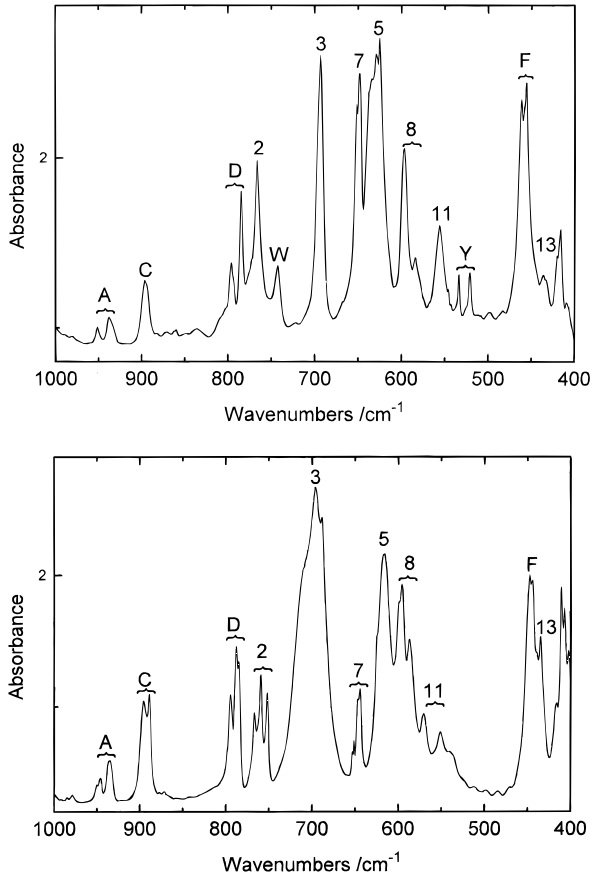

Figure 8. IR spectra (a, top) $[Mn_3O(OOCCMe_3)_6(py)_3]BF_4$ (**3**) and (b, bottom) $[Mn_3O(OOCCMe_3)_6(py)_3]$ (**4**) (KBr disks, $T = 80$ K; resolution 1 cm^{-1}).

Spectra of the oxidized (BF_4^- salt) and mixed-valence manganese complexes **3** and **4** are compared in Figure 8. (The BF_4^- salt was preferred to the ClO_4^- salt because a vibration of ClO_4^-

(20) Longueville, W.; Fontaine, H. *Mol. Cryst. Liq. Cryst.* **1976**, 32. Longueville, W.; Vergoten, G.; Fontaine, H. *J. Raman Spectrosc.* **1982**, *13*, 213.

(21) Long, G. J.; Robinson, W. T.; Tappmeyer, W. P.; Bridges, D. L. *J. Chem. Soc., Dalton Trans.* **1973**, 573.

(22) Wu, R.; Arap Koske, S. K.; White, R. P.; Anson, C. E.; Jayasooriya, U. A.; Cannon, R. D. *J. Chem. Soc., Chem. Commun.* **1994**, 1657.

obscures an important part of the spectrum—see Table 3, band X and footnote; no other significant differences were noted between the two spectra apart from the bands due to BF_4^-.) Apart from some small but important splittings, discussed below, the coordinated pyridine and pivalate modes are assigned as before and similar remarks apply. The expected broad bands for $\nu_{as}(Mn_3O)$ do not appear clearly in either of these spectra, but in a comparison of the absorption profiles with the corresponding parts of Figure 7 for the iron complexes, it seems clear that at least one broad band is concealed in the region of 600−650 cm^{-1} in the case of the trimanganese(III) complex and two well-separated bands in the regions of ca. 700 and ca. 600 cm^{-1} in the case of the mixed-valence manganese complex. The higher-frequency component was well resolved in the perdeuteriopyridine adduct of the mixed-valence manganese complex.

Discussion

The contrasting valency characters of the four oxotrimetal clusters are well shown by the IR spectra. In the fully oxidized triiron(III) and trimanganese(III) complexes the crystal structures show all three metal atoms to be distinct, but in the iron case the differences are evidently too small to be resolved in the spectra. In a comparison of Figures 7a and 8a, several ligand vibration bands which are single or barely resolved in the iron complex are clearly split in the manganese complex, notably bands 7 (pyridine ring deformation with substantial motion of the N atom), D and F (pivalate), and 8 (π-CO_2). In each case the splittings are small but well defined, and the split components are of unequal intensity.

The analogous bands in the mixed-valence manganese complex **4** (Figure 8b) are also all split, usually to a greater extent, and sometimes into three components of similar intensity. In most cases the splittings into two give components of unequal intensity (bands C and 7) and the splittings into three give components of unequal separation (bands A, 2, and 8). The implication is that the major difference between the manganese centers is that which is obvious from the crystal structure, i.e., one manganese of low valency and two of high valency, but the two isovalent manganese atoms are also different enough to affect the spectra and more so than the three isovalent manganese atoms in the trimanganese(III) complex. [One contribution to observed splitting may be intermolecular coupling. In an asymmetric space group such as $P2_12_12_1$ (Mn^{III}_3O, structure **2**), all four factor group components of any mode are IR-active, whereas, in a higher-symmetry group such as $P2_1/n$ (Fe^{III}_3O, structure **1**), only two of the four are IR-active. It is difficult to quantify this effect, but it is clear that the splittings we observe, some of which are large, give a self-consistent picture of the molecular symmetries.]

There is no doubt that in the mixed-valence manganese complex, and in the mixed-valence iron complex at sufficiently low temperature, the metal ion clusters consist of oxidation states ($M^{3+}M^{3+}M^{2+}$), with bond distances, angles, and vibrational frequencies characteristic of the two metals in the respective oxidation states. Above the phase transition, the iron complex can be described to a good approximation as ($Fe^{3+}Fe^{2.5+}Fe^{2.5+}$) but with two reservations: (1) The two sites denoted $Fe^{2.5+}$ are crystallographically distinct and therefore may also be slightly different in average oxidation state. (2) The time scale has to be carefully considered. The Mössbauer spectral transition is sharp, and there is no sign of lifetime broadening in the spectra on either side of the transition. However the time scale for measurable broadening is in the range 10^7−10^9 s^{-1}. Intramolecular electron-transfer processes could be envisaged in at least two ways as follows:

$$M^{2+} + 2M^{3+} \rightleftarrows M^{3+} + 2M^{2.5+} \quad (1)$$

$$M^{2+} + M^{3+} \rightleftarrows M^{3+} + M^{2+} \quad (2)$$

The first of these, if sufficiently rapid, would give the time-averaged state close to ($M^{2.67+}M^{2.67+}M^{2.67+}$), and there is no evidence of this in our data. The second would give (Fe^{3+}-$Fe^{2.5+}Fe^{2.5+}$), still subject to the reservation (1). The Mössbauer data are therefore consistent with sudden onset of process (2) at temperatures just above 100 K, the lowest rate constant after the onset being more than about 10^9 s^{-1}. This would mean that the rate of electron transfer has passed rapidly through the window of the Mössbauer time scale, though, as we argue below, it remains slower than the vibrational time scale. The room-temperature X-ray structure is consistent with this. (Though all comparisons between X-ray diffraction and spectroscopic data assume that the crystals studied by X-ray are representative of the powder samples.) The near equivalence of bonds to atoms Fe2 and Fe3 would suggest either valence delocalization or disordering of an adjacent pair of iron(III) and iron(II) centers. Between these two alternatives, the thermal ellipsoids favor disorder, since they are markedly anisotropic, in contrast to the ellipsoid of Fe1 which is close to isotropic. (Their long axes are roughly parallel to the Fe_3 plane and directed toward a point close to the central oxygen, on the side remote from Fe1). The Mössbauer data then imply that the disorder is dynamic rather static.

The symmetry implications of the IR spectra of the mixed-valence iron complex are more complicated, however. The large splitting of $\nu_{as}(Fe_3O)$ is similar to that seen in previous studies of mixed-valence acetate complexes[4] and is as expected for approximate 2-fold symmetry due to the nonequivalence of the iron atoms. The temperature dependences of the line widths and frequencies of metal−oxygen stretches have already been interpreted[22] on the basis of a thermal electron transfer, with an Arrhenius-type temperature dependence leading to a rate ca. 5×10^{11} s^{-1} at $T = 300$ K. The theory behind this interpretation is not straightforward, as the vibration being used to sense the electron transfer is either the same as, or closely related to, that of the motion along the relevant reaction coordinate.[25] But other vibrations are less strongly coupled to the motion of the central oxygen and may be taken as spectators, probing the time scale of the electron-transfer process. For example, $\nu_{as}(CO_2)$ (not shown) and ρ_r(*t*-Bu-CO_2), band 11, are both broader for the mixed valence than for the fully oxidized iron complex, but they are not split and other modes remain sharp, notably the locally symmetric modes of the coordinated carboxylate ions,

(23) (a) Kline, C. H.; Turkevich, J. *J. Chem. Phys.* **1944**, *121*, 300. (b) Corrsin, L.; Fax, B. J.; Lord, R. C. *J. Chem. Phys.* **1953**, *21*, 1170. (c) Long, D. A.; Murfin, F. S.; Hales, J. L.; Kynaston, W. *Trans. Faraday Soc.* **1957**, *53*, 1171. (d) Wilmshurst, J. K.; Bernstein, H. J. *Can. J. Chem.*. **1957**, *35*, 1183. (e) Green, J. H. S.; Kynaston, W.; Paisley, H. M. *Spectrochim. Acta* **1963**, *19*, 549. (f) Long, D. A.; Murfin, F. S.; Thomas, E. L. *Trans. Faraday Soc.* **1963**, *59*, 12. (g) Long, D. A.; George, W. O. *Spectrochim. Acta* **1963**, *19*, 1777. (h) Wong, K. N.; Colson, S. D. *J. Mol. Spectrosc.* **1984**, *104*, 129.

(24) Gill, N. S.; Nuttall, R. H.; Scaife, D. E.; Sharp, D. W. A. *J. Inorg. Nucl. Chem.* **1961**, *18*, 79. Akyüz, S.; Dempster, A. B.; Davies, J. E. D.; Holmes, K. T. *J. Chem. Soc., Dalton Trans.* **1976**, 1746, supplementary Tables 2−5 (SUP 21804, 9 pp, from the Royal Society of Chemistry).

(25) Turner, J. J.; Gordon, C. M.; Howdle, S. M. *J. Phys. Chem.* **1995**, *99*, 17532.

(26) Nakamoto, K. *Infrared and Raman Spectra of Inorganic and Coordination Compounds*: 4th ed.; John Wiley and Sons: New York, 1986.

$\nu_s(CO_2)$, and the pyridine modes 2 and 7. The standard deviations $D(\nu)$ of the frequencies of the components of these two modes, in the mixed-valence manganese complex, are about 7 and 5 cm^{-1}, respectively. If these are taken as measures of the splittings that would have been observed for a fully-localized ($2Fe^{3+} + Fe^{II}$) complex, and if the absence of splitting is attributed to a time-dependent delocalization process process, the rate of this process can be estimated, as a lower limit, $\tau^{-1} = D(\nu) \times c = 2 \times 10^{11}$ s^{-1}, which is consistent with the previous estimate.

Conclusions

The main concern of this study was to establish the electronic character of the two mixed-valence triangular complexes. These pivalate-bridged complexes have proved ideal for the purpose: In each of them the lattice symmetry (at room temperature) is such that there is just one crystallographically distinct type of molecule and no imposed internal symmetry, so that all metal−ligand bonds and angles are independently determined. Moreover the metal clusters are relatively well separated and there are no obvious pathways for intermolecular electronic coupling. This is particularly relevant in the case of the mixed-valence iron cluster. The three pyridine molecules are essentially coplanar with the triiron cluster, but they are not parallel to those of neighboring molecules and the closest intermolecular approach distance is 6 Å. This contrasts with the mixed-valence acetato complex, in which the molecules are stacked in columns with pseudo-3-fold symmetry, the coordinated pyridines are similarly stacked, and distances between adjacent rings are close to those of direct contact (3.65 Å;[8] cf. the interplanar spacing in graphite, 3.4 Å[10]). As noted above, various numbers of *tert*-butyl groups are rotationally disordered, the angles between coordinated pyridine molecules and the trimetal atom planes vary widely, and none of these features relate in any obvious way to the approximate symmetries of the central M_3O clusters. All these features give us confidence that the properties of the central clusters reflect their intrinsic electronic structures and are not strongly influenced by external packing forces.

As regards the valence delocalization seen in the iron mixed-valence complexes, the data reinforce the findings from other studies of complexes of the same structural type that at the lowest temperatures full valence localization is the norm and that with increasing temperature the onset of delocalization involves sharp phase transitions and therefore some degree of cooperativity. But as is now increasingly recognized, the delocalization process is dynamic. It is not solely a matter of valence averaging due to mixing of atomic electron wave functions but involves activated transfer of electronic charge between trapped-valence sites.

Acknowledgment. This work was supported by the Science and Engineering Research Council and the Ministry of Education, Science and Culture of Japan (Grant-in-Aid for Scientific Research No. 07554061).

Supporting Information Available: Tables S1−S4, listing atomic coordinates (with equivalent isotropic displacement parameters), bond lengths and angles, anisotropic displacement parameters, and hydrogen coordinates (with isotropic displacement parameters) for $[Fe_3O(O_2CCMe_3)_6(py)_3](ClO_4)\cdot 0.5py$; Tables S5−S8, similarly for $[Mn_3O(O_2CCMe_3)_6(py)_3](ClO_4)\cdot MeCN$; Tables S9−S12, similarly for $[Mn_3O(O_2CCMe_3)_6(py)_3]$; Table S13, listing atomic coordinates, equivalent isotropic displacement parameters, and site occupancy factors for $[Fe_3O(O_2CCMe_3)_6(py)_3]$; Tables S14−S17, listing bond lengths, bond angles, anisotropic displacement coefficients, and hydrogen coordinates (with isotropic displacement coefficients) for $[Fe_3O(O_2CCMe_3)_6(py)_3]$; and Table S18, listing Mössbauer spectral parameters (isotope shifts, quadrupole splitting parameters, intensities, bandwidths, areas) for $[Fe_3O(O_2CCMe_3)_6(py)_3]$ (40 pages). Ordering information is given on any current masthead page.

IC970451T